Electric dipole echoes and noise-induced decoherence

Journal of Physics: Conference Series **88** (2007) 012055 doi:10.1088/1742-6596/88/1/012055

Electric dipole echoes and noise-induced decoherence

J J Mestayer[1], W Zhao[1], J C Lancaster[1], F B Dunning[1,*], S Yoshida[2], C O Reinhold[3] and J Burgdörfer[2]

[1] Department of Physics and Astronomy, Rice University, Houston, Texas 77005, USA

[2] Institute for Theoretical Physics, Vienna University of Technology, A1040 Vienna, Austria, EU

[3] Physics Division, ORNL, Oak Ridge, Tennessee 37831, USA

E-mail: fbd@rice.edu

Abstract. The generation of echoes in the electric dipole moment of a Rydberg wavepacket precessing in an external electric field by reversal of the field is described. When the wavepacket experiences reversible dephasing, large echoes are observed pointing to strong refocusing of the wavepacket. The presence of irreversible dephasing leads to a reduction in the size of the echoes. The effect of irreversible dynamics on echoes is investigated using artificially synthesized noise. Methods to determine the decoherence rate are discussed.

Over the years a variety of echo phenomena have been observed and used to address questions related to reversible and irreversible dephasing, classical-quantum correspondence, and the coherent control and manipulation of quantum systems. For example, spin echoes form the basis of NMR spectroscopy [1], photon echoes provide a means to store single-photon wavepackets [2], and the Loschmidt echo probes the sensitivity of quantum wavepackets to perturbations [3]. Recently, the generation of echoes in the electric dipole moment of a high-n (n~350) Rydberg wavepacket has been demonstrated [4]. High-n atoms provide a valuable mesoscopic laboratory to explore concepts and technologies related to quantum information processing and coherent control [5-7]. While the precession of the electric dipole moment is similar in many respects to that of its magnetic counterpart, realization of an echo in the electric dipole moment is more challenging because of the shorter timescales associated with electronic orbital and precessional motion and of the strong coupling to the environment which can lead to rapid decoherence.

Here wavepackets comprising a mix of high-lying Stark states with n ~ 350 are produced by sudden application of a transverse dc field to quasi-one-dimensional (quasi-1D) n = 350 Rydberg atoms. Their subsequent precession about this field is monitored using a half-cycle probe pulse. Echoes are induced by reversing the direction of the applied field. At n ~ 350 the electron binding energy E = ($-1/2n^2$ a.u.) is ~110 μeV and the classical electron orbital period T_n (= $2\pi n^3$ a.u.) is ~6.5 ns. (Atomic units are used unless otherwise stated.) Classically, the electron orbit can be characterized by the energy E, the angular momentum $\boldsymbol{L} = \boldsymbol{r}\times\boldsymbol{p}$, and the Runge-Lenz vector $\boldsymbol{A} = \boldsymbol{p}\times\boldsymbol{L}-\boldsymbol{r}/r$ which determine its size, eccentricity, and orientation respectively. In a field $\boldsymbol{F}$, $\boldsymbol{L}$ and

[*] To whom all correspondence should be addressed.

A precess. If F is small, however, the orbit changes slowly compared to the time scale T_n whereupon it can be considered as a dynamical entity whose behaviour can be discussed in terms of the orbit-averaged quantities $\langle \boldsymbol{L} \rangle$ and $\langle \boldsymbol{A} \rangle$ using the pseudo-spins $\boldsymbol{J}_\pm \equiv (\langle \boldsymbol{L} \rangle \pm n \langle \boldsymbol{A} \rangle)/2$. To first order in F, $\boldsymbol{J}_\pm$ evolve according to two decoupled Bloch equations

$$\frac{\mathrm{d}}{\mathrm{dt}} \boldsymbol{J}_\pm = \omega_\pm(\mathrm{F}) \boldsymbol{J}_\pm \times \hat{\boldsymbol{z}} \qquad (1)$$

and precess about the field (taken to define the z axis) with angular velocities $\omega_\pm \sim \pm 3nF/2$ ($\equiv \omega_\pm^{(1)}$) much like the spin precession in a magnetic field (see insert in figure 1). However, the magnitude of the electric dipole moment (proportional to $\langle \boldsymbol{A} \rangle = (\boldsymbol{J}_+ - \boldsymbol{J}_-)/n$) changes periodically in time oscillating at the Stark frequency $\omega_s = 2\omega_+^{(1)}$ which corresponds to the hydrogenic Stark frequency splitting within the n manifold. A Rydberg wavepacket comprising states with different values of n will possess a range of precession frequencies $\omega_\pm(F,n)$ (or equivalently $\omega_s(n)$). Thus, even if the initial phases of the pseudo-spins are well localized this will lead to dephasing of the wavepacket. Such dephasing can be reversed by reversing the applied field $F \rightarrow -F$ (and thus the direction of precession) leading to the generation of a strong echo [4]. By periodically reversing the applied field the wavepacket can rephase repetitively and generate a series of closely spaced echoes. The complete reversibility of the dynamics implied by equation (1) is destroyed by coupling to the Kepler motion (see below) or by the presence of inhomogenities in the applied field, both of which lead to a reduction in the size of the echoes. The effects of such irreversible dephasing can be examined by application of noise. In an ensemble of Rydberg atoms dipole-dipole interactions can induce stochastic forces that can be interpreted as a source of noise.

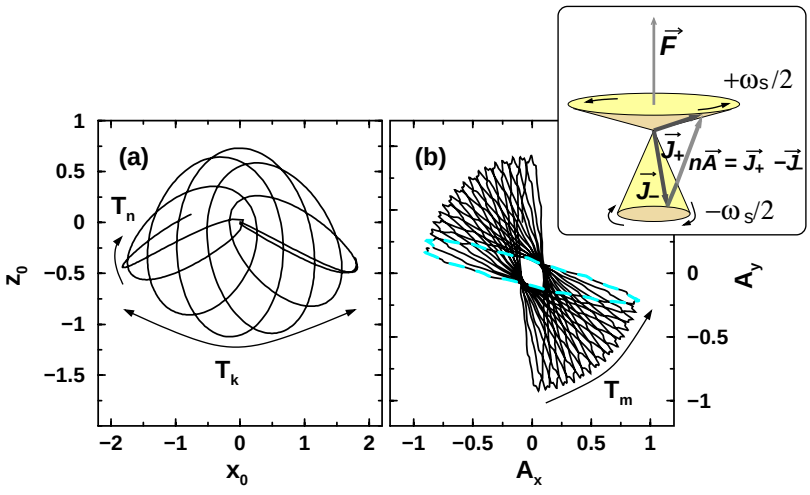

Figure 1. Time evolution of the classical Rydberg electron trajectory (n = 350) in a field F = 2 V m^{-1} directed along the z axis. (a) projection of the trajectory onto the (x,z) plane during a Stark precession period $T_S \sim 40$ ns. (b) slow rotational motion in the (A_x,A_y) plane for $0 \le t \le 1$ μs ($T_m \sim 2.5$ μs). The whole trajectory in (a) is projected onto the highlighted single ellipse in (b). All coordinates are in scaled units ($r_0 = r/n^2$, $p_0 = np$). The inset shows the behaviour of the pseudo-spins $\boldsymbol{J}_\pm$, which to first order precess with angular velocities $\pm\omega_S/2$.

In an electric field, a typical Rydberg electron trajectory (figures 1a, 1b) embodies motion on three different timescales. The electron orbits rapidly on an approximate Kepler ellipse with period T_n. This ellipse precesses in the field and undergoes oscillations in eccentricity on an intermediate time scale $T_k \sim 2T_s = 4\pi/\omega_s$. Such Stark precession results in an elliptic trajectory of the Runge-Lenz vector in the (A_x,A_y) plane (figure 1b). This trajectory rotates slowly about the A_z-axis with period T_m. These three time scales can be derived from the hydrogenic eigenenergies, given to second order in F by

$$E_{n,k,m} = -\frac{1}{2n^2} + \frac{3}{2}nkF - \frac{1}{16}n^4[17n^2 - 3k^2 - 9m^2 + 19]\,F^2 \qquad (2)$$

where k and m are the electric and magnetic quantum numbers. Expressing the classical energy in terms of the z components of the pseudo-spins, $J_{\pm}^{z} = (m \pm k)/2$, the precession frequencies become

$$\omega_{\pm}(F) = \frac{\partial E(n, J_{+}^{z}, J_{-}^{z})}{\partial J_{\pm}^{z}} = \pm(\omega_k^{(1)}(F) + \omega_k^{(2)}(F)) + \omega_m^{(2)}(F) \qquad (3)$$

where $\omega_k^{(1)}(F) = 3nF/2$ is the first-order angular velocity, and $\omega_k^{(2)}(F) = (3/8)n^4kF^2$ and $\omega_m^{(2)}(F) = (9/8)n^4mF^2$ are the second-order corrections. $\omega_m^{(2)}$ determines the rotation period $T_m (= 2\pi/\omega_m^{(2)})$ and lifts the degeneracy between the magnitudes of the rotation frequencies ω_+ and ω_-. Since $\omega_m^{(2)}$ is identical for both pseudo-spins it can be separated from the Stark precession by transforming into a frame rotating with this angular velocity. In this primed frame the Bloch equations become [4]

$$\frac{d}{dt}\boldsymbol{J}_{\pm}' = \pm\omega_k(F)\boldsymbol{J}_{\pm}' \times \hat{\boldsymbol{z}} \qquad (4)$$

with $\omega_k(F) = \omega_k^{(1)}(F) + \omega_k^{(2)}(F)$, $\boldsymbol{J}_+'$ and $\boldsymbol{J}_-'$ having the common precession period $T_k = 2\pi/\omega_k(F)$. While the reversal of the field will lead to a reversal in the direction of precession, the presence of the second-order term in $\omega_k(F)$, i.e. the coupling between the Stark precession and the Kepler motion, will result in a change in the precession rate limiting the degree of rephasing that can be achieved.

In the present experiments, quasi-1D Rydberg atoms oriented along the x axis are first created by selectively photoexciting ground-state potassium atoms to a mix of the lowest-lying red-shifted states in the n = 350 Stark manifold in a weak (~25 mV m^{-1}) dc field directed along the x axis [8]. A much larger dc field F = 2 V m^{-1} is then suddenly applied (rise time ~0.3 ns << T_n) in the z direction to create a wavepacket comprising a coherent superposition of Stark states with a narrow range of n, and small values of k. Because k is small, the effect of the second-order term $\omega_k^{(2)}$ is reduced. The field can be reversed F $\rightarrow$ -F as required, the switching time $t_s \sim 10\text{ns} \sim T_n$ being selected to effectively prevent transitions between states of different n and avoid additional line broadening. The evolution of the wavepacket is monitored using a probe half-cycle pulse (HCP), of duration $T_p \sim 0.6$ ns and amplitude sufficient to ionize ~50% of the atoms, that is applied along the z axis after a variable time delay. Because the probe HCP is very short, $T_p << T_n$, it simply delivers an impulsive momentum transfer $\boldsymbol{\Delta p}$ to the electron. The resulting energy transfer depends on the initial z component of electron momentum. The overall survival probability, measured by field ionization, therefore maps the variation in the orientation and elongation, i.e., eccentricity ε (= $|\boldsymbol{A}|$), of the Kepler ellipse – the "Stark beats" of the electric

dipole moment [4]. Since the probe HCP is applied along the z axis, irreversible dephasing induced by the second order term $\omega_m^{(2)}$ is suppressed.

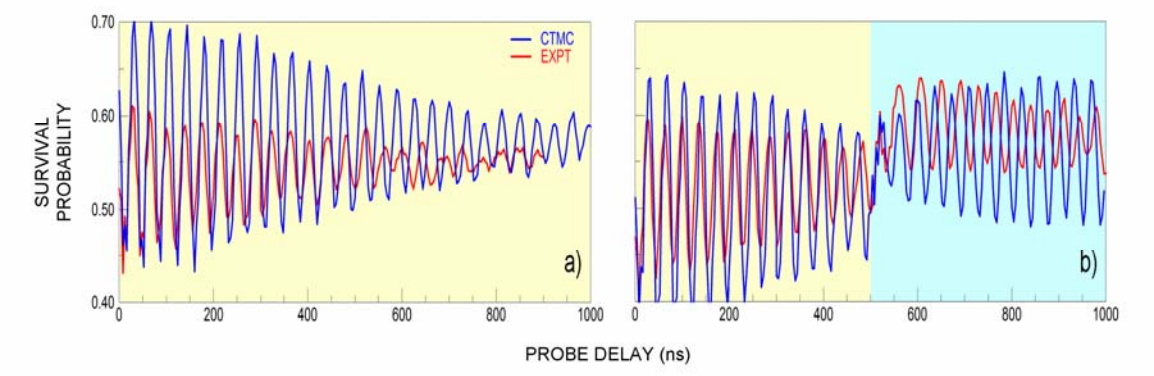

Figure 2. Time-resolved survival probabilities with: (a) no field reversal; (b) field reversal at $t = \tau = 500$ ns. The initial mix of x-oriented Stark states is subject to sudden application of a field $F = 2$ V m^{-1} along the z-axis. The probe pulse strength is $\Delta p = -0.536/n$ (a.u.).

As illustrated in figure 2a, without field reversal the amplitude of the Stark beats decreases monotonically with time due to dephasing. Similar behaviour is predicted by classical trajectory Monte Carlo (CTMC) simulations in which a microcanonical ensemble of points in phase space is used to represent the initial mix of Stark states (see figure 2a). The ensemble of points is propagated in time according to Hamilton's equation of motion. The differences in the amplitude and period of the beats can be attributed to uncertainties in the exact mix and orientation of the initial states and in the size of the applied field, F. Reversal of the field at $t = \tau = 500$ ns results in the appearance of a strong echo at $t = 2\tau$ (see figure 2b). This indicates that, because the higher-order terms are small, a significant fraction of the dephasing is reversible. The relative size of the observed echo, however, is somewhat smaller than calculated providing evidence of irreversible dephasing beyond that associated with $\omega_k^{(2)}$ (which is taken into account in the CTMC simulations). Note that when the probe pulse is applied before $t = 500$ ns higher n states are excited which do not respond adiabatically to field reversal leading to ionization and a reduction in the survival probability.

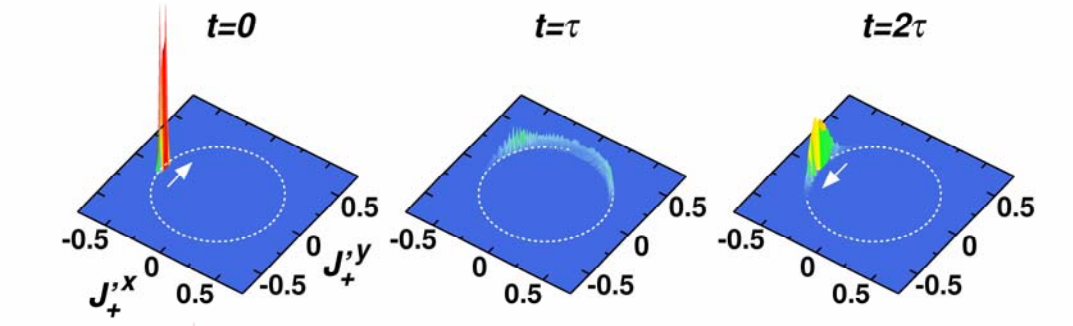

Figure 3. Snapshots showing the calculated time evolution of the probability density in the $J_+'^x$, $J_+'^y$ plane for the lowest-lying state in the $n = 350$ Stark manifold (see text). The snapshots are taken at $t = 0$, τ, and 2τ, where $\tau = 500$ ns. The arrows denote the precessional motion. The pseudospins are expressed in scaled units.

The dephasing and subsequent rephasing of the wavepacket can be seen clearly in the time evolution of the probability density of the pseudospins. This is illustrated in figure 3 for the extreme red-shifted state in the n = 350 Stark manifold, i.e., the state with the largest initial polarization. The precessional motion (equation 4) proceeds around the circle shown and the sense of rotation is reversed after the field is reversed. The probability density is initially strongly localized in azimuthal angle $\phi = \arctan(J_+'^y/J_+'^x)$ and centered near $\phi=\pi$. It evolves around the circle and spreads as it dephases. After field reversal the wavepacket rephases leading to an echo at $t=2\tau$.

In figure 4 dephasing of the present initial state is quantified by considering the time evolution of the calculated width $\langle(\Delta\phi^2)\rangle^{1/2}$ of the azimuthal angle distribution of the pseudospins. To emphasize the growth in the azimuthal width, the initial width is subtracted from the total width, i.e. $\langle\Delta\phi\rangle = (\langle(\Delta\phi(t))^2\rangle - \langle(\Delta\phi(t=0))^2\rangle)^{1/2}$. Without field reversal the width increases linearly in time due principally to the spread in the first-order precession frequencies $\omega_k^{(1)}$. Upon field reversal the width decreases as the echo builds but does not recover its initial value, rather it falls to a minimum value determined by the (irreversible) second-order term $\omega_k^{(2)}$ whereupon it again begins to increase. The position of the minimum provides a measure of the irreversible dephasing rate, which is seen to be about one quarter of the total dephasing rate.

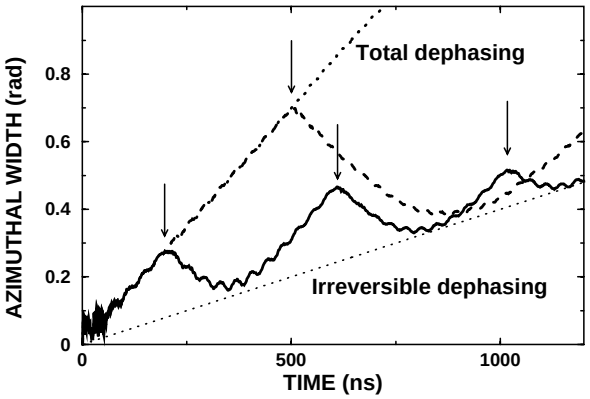

Figure 4. Calculated time evolution of the azimuthal width $\langle\Delta\phi\rangle$ (see text). The times of field reversal are indicated by arrows. The other conditions are the same as for figure 2.

As seen in figure 4, repetitive field reversals can be used to restrict and control the amount of dephasing by producing a series of closely-spaced echoes. The degree of refocusing that can be achieved, however, remains limited by irreversible dephasing. Experimental data showing the effect of multiple reversals are presented in figure 5(a). The quantum beats persist largely unchanged for an extended period indicating that irreversible dephasing is slow. It is, however, difficult to extract azimuthal widths from the experimental data to determine dephasing rates. Work is in progress to develop a more practical measure of the dephasing rate using a wavelet analysis scheme that localizes the frequency spectrum in time.

The irreversible dephasing induced by the second-order corrections can be further enhanced by stochastic interactions with the environment. To explore this, noise was injected by randomly modulating the amplitude of the dc field using the output of a pulse pattern generator which

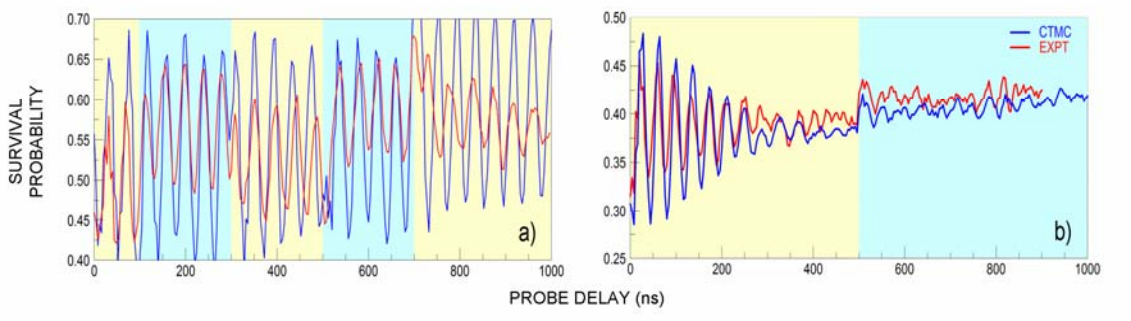

Figure 5. Time-resolved survival probabilities with using the same initial state and field and probe pulse strengths as in figure 2: (a) field reversal at 100, 300, 500, and 700 ns; (b) field reversal at t = 500 ns but with noise of amplitude $\Delta F = \pm 0.1F$ (see text);

divides time into a series of bins of equal width and in each randomly outputs a high or low voltage level. A bin width of 2 ns was selected because the corresponding peak in the noise power spectrum matches the electron orbital frequency leading to enhanced dephasing [9]. As seen in figure 5(b), the presence of noise with an amplitude of only ± 10% of that of the dc field results in rapid damping of the quantum beats. No significant echo is observed, or predicted by simulations, following field reversal showing that this noise level is sufficient to irreversibly dephase the initial state on a sub-microsecond time scale.

Stark quantum beat echoes demonstrate the time-reversibility of the electric dipole precession about a static field and provide a powerful probe of both reversible and irreversible dephasing in mesoscopic quantum systems. The technique can be applied on time scales much shorter than those associated with revivals allowing measurements even in the presence of very strong dephasing. Given that it is possible to synthesize controlled coloured (rather than "white") noise the role of its spectral distribution on dephasing can be explored. Because decoherence induced by noise converts a coherent superposition of states into an incoherent statistical mixture, the present technique promises new insights into how noise drives the transition from quantum to classical behaviour [10].

Acknowledgments
Research supported by the FWF (Austria), the US DoE, the NSF and the Robert A Welch Foundation. The help of B. Wyker in data acquisition is also appreciated.

References
[1] Hahn E L, 1950 *Phys. Rev.* **80** 580
[2] Abella I D, Nurnit N A and Hartmann S R, 1966 *Phys. Rev.* **141** 391
[3] Jalabert R A and Pastawski H M, 2001 *Phys. Rev. Lett.* **98** 2490
[4] Yoshida S, Reinhold C O, Burgdörfer J. Zhao W, Mestayer J J, Lancaster J C and Dunning F B, 2007 *Phys. Rev. Lett.* **98** 203004
[5] Ahn J, Weinnacht T C and Bucksbaum P H, 2000 *Science* **287** 463
[6] Maeda H, Norum D V L and Gallagher T F, 2005 *Science* **307** 1757
[7] Minns R S, Kutteruf M R, Zaidi H, Ko L and Jones R R, 2006 *Phys. Rev. Lett.* **97** 040504
[8] Dunning F B, Lancaster J C, Reinhold C O, Yoshida S and Burgdörfer J, 2005 *Adv. At. Mol. Opt. Phys.* **54** 49-103
[9] Yoshida S, Reinhold C O, Burgdörfer J, Zhao W, Mestayer J J, Lancaster J C and Dunning F B, 2007 *Phys. Rev.* A **75** 013414
[10] Gardiner C W, Zoller P, 1999 *Quantum Noise* (Springer, NY)